Inverse design in the complex plane: Manipulating quasinormal modes

J. R. Capers,* D. A. Patient,† and S. A. R. Horsley
Department of Physics and Astronomy, University of Exeter, Stocker Road, Exeter EX4 4QL, United Kingdom

(Received 27 July 2022; accepted 10 November 2022; published 28 November 2022)

Utilizing the fact that the frequency response of a material can be decomposed into the quasinormal modes supported by the system, we present two methods to directly manipulate the complex frequencies of quasinormal modes in the complex plane. We first consider an "eigenpermittivity" approach that allows one to find how to shift the permittivity of the structure everywhere in order to place a single quasinormal mode at a desired complex frequency. Secondly, we then use perturbation theory for quasinormal modes to iteratively change the structure until a given selection of quasinormal modes occurs at desired complex frequencies.

DOI: 10.1103/PhysRevA.106.053523

I. INTRODUCTION

Quasinormal modes (QNMs) are the complex frequency bound states of a system. They were first used in quantum mechanics to describe alpha decay [1,2], and have since found utility in modeling radiation in many different systems, from black holes [3] to photonic resonators [4] to leaky waveguides [5,6]. QNMs correspond to the poles of the scattering matrix in the complex frequency plane [7,8], where the waves at the boundary of the system are purely outgoing. The effect of a structured environment can, for example, be analyzed by decomposing the Purcell factor in terms of these QNMs [9], and through calculating how small changes in the system perturb the QNMs deeper insight into sensing has been developed [10,11]. Here, motivated by the connection between the location of poles in the complex plane and physical properties such as transmission, we combine ideas from inverse design with the QNM approach to modeling resonator systems to design materials that have poles at specific complex frequencies. Perhaps the simplest example of a system supporting QNMs is a homogeneous dielectric slab (refractive index n_R in some background index n_B). For this simple case, the complex frequencies of the QNMs can be found analytically [3,4] as

$$k_m L = \frac{2\pi m + i \ln[(n_R - n_B)^2/(n_R + n_B)^2]}{2n_R}, \tag{1}$$

where m is an integer and L is the width of the slab. Figures 1(a)–1(c) demonstrate that poles in the reflection coefficient as a function of complex k correspond to QNMs, which are in turn associated with peaks in transmission. Examining the field, shown in Fig. 1(c), at a complex k value associated with a QNM shows the characteristic exponential growth in space.

More complicated systems can also be understood in terms of QNMs. For example, multilayer dielectric absorbers (e.g., the midinfrared absorber presented in [12]) can be understood this way. The absorption of the structure given in [12], along with the reflection coefficient in the complex wavelength plane, are shown in Figs. 1(d) and 1(e). Fitting the Lorentzian

$$\mathcal{L}(\lambda) = \frac{\Gamma}{(\lambda - \lambda_0)^2 + \Gamma^2} \tag{2}$$

to the absorption peak, we find the peak wavelength is $\lambda_0 = 5.15\ \mu\text{m}$ and the linewidth $\Gamma = 0.0138\ \mu\text{m}$. This corresponds to a pole of the reflection coefficient in the complex plane at $\lambda_0 + i\Gamma$, as shown in Fig. 1(e).

While QNMs provide a valuable framework to understand resonators, the ability to *design* the spectral response of materials is key to, e.g., more efficient photovoltaic cells [13] and sensors [14]. For sensing applications, narrow resonances at particular wavelengths are desirable [15–17], while energy harvesting requires large absorption over a broad band [18–21].

When designing spectral features, one can employ the physical insight provided by QNMs to greatly simplify the problem. For example, one way to approach the inverse design problem for absorbers is to try to move the QNM to a desired complex frequency [22]. In this way, one can tailor scattering effects [23], design absorbers [24], and manipulate exceptional points [25] with minimal numerical complexity. To date, however, these approaches address the forwards problem, finding how the pole moves if the resonator geometry is changed. We instead solve the inverse design problem of designing materials with poles at specific complex frequencies, using only simple techniques.

We present two methods for placing QNM poles at arbitrary complex frequencies. First, we reformulate the eigenvalue problem of the Helmholtz equation to find a complex constant value by which the permittivity of a structure should be shifted to place a pole in the desired location. Secondly, we employ QNM perturbation theory to find how to change the spatial distribution of material to move around several poles in the complex frequency plane. These methods enable the simultaneous control of resonance wavelength *and* linewidth, for the design of absorbers and sensors.

*jrc232@exeter.ac.uk
†dp348@exeter.ac.uk

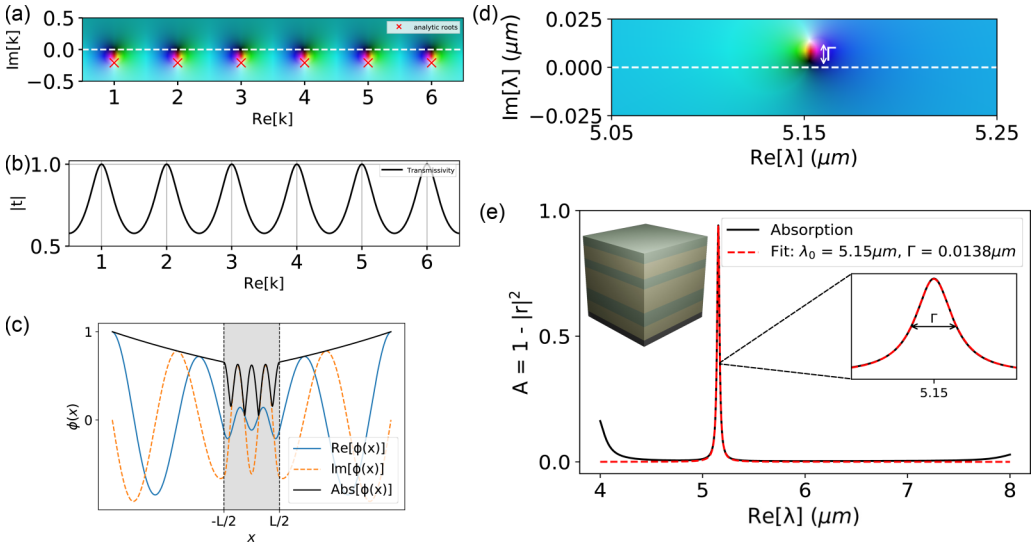

FIG. 1. The quasinormal modes of a dielectric slab (a–c) and the absorbing stack (d, e). The reflection coefficient in the complex plane is shown in panel (a) and transmission ($\sqrt{1-|r|^2}$) along the real frequency axis is shown in panel (b). The red crosses represent the analytic solution to Eq. (1) for $n_b = 1$, $n_r = \pi$, and $L = 1$. The real components of the QNMs are associated with the peaks in transmission. The real (blue), imaginary (orange dashed), and absolute (black) field distribution (c) of the $m = 3$ mode is shown to have the characteristic exponential growth in space. For the (near) perfect absorber (depicted in the inset: green layers are germanium and yellow are silicon oxide, with a tungsten substrate), the complex reflection coefficient (d) shows a single QNM. The absorption spectrum (e) shows a large resonance in the mid-IR, with a resonant frequency (λ_0) and linewidth (Γ) directly associated with the QNM, which can be understood in terms of the poles of the associated Lorentzian (red dashed line).

II. EIGENPERMITTIVITIES

One way to *find* the locations of QNMs is to formulate the Helmholtz equation for the out-of-plane electric field ϕ, as an eigenvalue problem for complex wave numbers k:

$$-\frac{1}{\varepsilon(x)}\frac{d^2\phi}{dx^2} = k^2\phi. \tag{3}$$

However, to find the QNMs the correct boundary condition must be imposed on ϕ. Originally derived by Sommerfeld [26], but since used to model black-hole radiation [27,28], the appropriate boundary condition is that the wave is purely outgoing. For example, on either side of a planar medium,

$$\frac{d\phi(x)}{dx} = \pm ik\phi(x), \tag{4}$$

as $x \to \pm\infty$. To numerically find the QNMs of our system, we imposed this boundary condition within a finite difference approximation, adapting the elements of the Laplacian at the boundaries; e.g., for N points the value of the field at the final point on the right of the system is fixed to be $\phi_{N+1} = \phi_N + ik\Delta x\phi_N$, giving

$$\frac{d^2\phi}{dx^2} \approx \frac{1}{(\Delta x)^2}\begin{pmatrix} (ik\Delta x - 1) & 1 & 0 & 0 \\ 1 & -2 & 1 & 0 \\ 0 & 1 & -2 & 1 \\ 0 & 0 & 1 & (ik\Delta x - 1) \end{pmatrix} \times \begin{pmatrix} \phi_1 \\ \phi_2 \\ \phi_3 \\ \phi_4 \end{pmatrix}. \tag{5}$$

It is now evident that solving the eigenvalue problem required to find the QNMs is challenging [29] as the eigenvalue k^2 also appears in the boundary condition. To avoid solving this nonlinear problem, it has recently been noted by Chen *et al.* [30] that the analysis of QNMs can be simplified by working in terms of real wave numbers but extending the *permittivity* into the complex plane. Despite the utility of the normal-mode framework of Chen *et al.* for employing modal expansions we are trying to engineer the resonance location (related to Re[k]) and linewidth (given by Im[k]). The location of the QNM frequency trivially encodes these features we are trying to engineer. Employing the insight of Chen *et al.*, we write the permittivity as a spatial variation plus a constant background $\varepsilon(x) = \varepsilon_s(x) + \varepsilon_b$ that allows us to recast the Helmholtz equation as an eigenvalue problem for the permittivity:

$$-\frac{1}{k^2}\left(\frac{d^2}{dx^2} + k^2\varepsilon_s(x)\right)\phi(x) = \varepsilon_b\phi(x). \tag{6}$$

Rather than using this to find the QNMs of a system, we show that this can be used to design the complex frequencies of the QNMs.

To do this, we take a known spatially varying permittivity, such as the dielectric step or absorber stack, e.g., from [12], and choose a $k \in \mathbb{C}$ at which we would like a QNM to occur. We then numerically solve the eigenvalue problem Eq. (6) using the finite difference method Eq. (5), along with standard matrix libraries, to find a complex eigenpermittivity that allows us to form a structure with $\varepsilon(x) = \varepsilon_s(x) + \varepsilon_b$ with a pole at the chosen complex frequency.

We first apply the method to the homogeneous slab. In Fig. 2 we design the new structure to support a QNM at the frequency $k = 1.5 - 0.05i$. For the $N \times N$ Laplacian

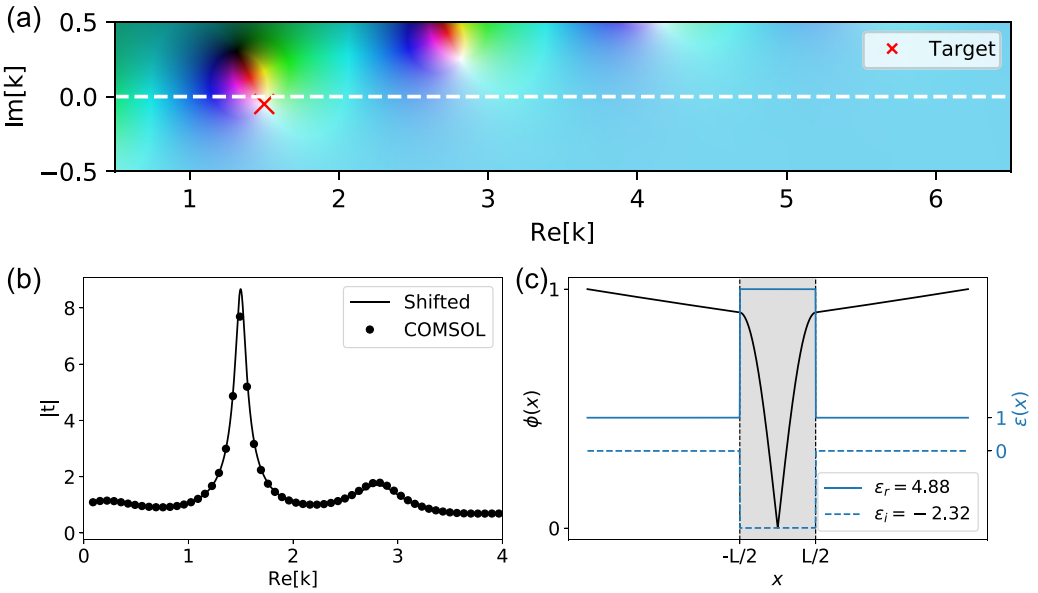

FIG. 2. A background permittivity $\varepsilon_b = -4.99 - 2.32i$ is found as a solution to Eq. (5) which, when combined with the original structure $\varepsilon_s(|x| < L/2) = \pi^2$, will contain a pole at the desired complex frequency of $k = 1.5 - 0.05i$. The reflection coefficient of the new structure is plotted in the complex plane (a). The transmission along the dashed white line, where Im[k] = 0 is plotted (b), is shown alongside the field distribution plotted at the complex frequency k (c). Overlaid on the transmission calculations are results found using COMSOL MULTIPHYSICS [31].

matrix, there are N possible values for ε_b that will satisfy this condition. Taking the lowest absolute valued background (to minimize numerical error) permittivity $\varepsilon_b = -4.99 - 2.32i$, we find that the new structure now supports a QNM at our chosen k. This is shown in Fig. 2(a). The transmission, Fig. 2(b), shows a large peak at the real frequency associated with the QNM and has values $|t| > 1$ due to the gain that has been added to the system. Although the location of the pole can be manipulated solely by changing the height of the barrier, in order to manipulate the real and imaginary parts independently, control over both the real and imaginary permittivity is required. As might be anticipated, in order to move a pole closer to the real frequency axis, without changing the resonant frequency, gain is required. Conversely, loss is required to move the pole further away from the real axis. The field profile, shown in Fig. 2(c), still has the exponential growth characteristic of QNMs.

Next, we apply the same eigenpermittivity method to the absorbing stack shown in Fig. 1(e). For this structure, we must take care that the correct boundary conditions are imposed. The opaque metal substrate requires the Dirichlet boundary condition $\phi = 0$, while the outgoing wave boundary condition must be imposed at the top of the stack. Choosing two target bandwidths, for the same resonance wavelength, $\lambda_1 = (6.5 + 0.03i)$ μm and $\lambda_2 = (6.5 + 0.15i)$ μm, we obtain background permittivities of $\varepsilon_{b,1} = 3.27 - 0.01i$ and $\varepsilon_{b,2} = 3.28 + 0.29i$. The effect of the background shift on the pole locations is shown in Figs. 3(a) and 3(b). Accordingly, the poles are found at the expected complex frequencies. The absorption, shown in Fig. 3(c) plotted along the white dashed line (Im[λ] = 0), is also provided, with a fitted Lorentzian to extract the properties of the resonances and verify that they correspond to the QNM frequencies.

We can also apply this design procedure to impose the condition of coherent perfect absorption (CPA) at a given complex frequency. This can be understood as the time reverse of QNMs [32] where the wave is purely incoming rather than outgoing. The wavelengths at which a structure behaves as a perfect absorber are related to the locations of zeros on the real axis, rather than poles. With our eigenpermittivity formulation, we can find the background permittivity value required to make the device a perfect absorber at a frequency of choice. To do this, we simply take the outgoing boundary condition Eq. (4) and replace it with the incoming boundary condition

$$\frac{d\phi(x)}{dx} = \mp ik\phi(x) \tag{7}$$

as $x \to \pm\infty$. This changes the boundary elements in the Laplacian Eq. (5) from $ik\Delta x - 1$ to $-ik\Delta x - 1$.

Applying the above changes to the Laplacian matrix, we can take, e.g., a slab of dielectric, and rather than choose a complex frequency pick a real frequency that we wish CPA to occur at. We take a dielectric slab of length $L = 1$ and initial permittivity π^2 and choose the arbitrary CPA frequency to be 125 MHz. The resulting background permittivity required is $\epsilon_b = -9.55 + i0.63$. To verify that there is coherent perfect absorption at the chosen frequency, we construct the scattering matrix for the slab under incidence from the left and right side:

$$\begin{pmatrix} \phi_L^{\text{scattered}} \\ \phi_R^{\text{scattered}} \end{pmatrix} = \begin{pmatrix} r_L & t_R \\ t_L & r_R \end{pmatrix} \begin{pmatrix} \phi_L^{\text{in}} \\ \phi_R^{\text{in}} \end{pmatrix}, \tag{8}$$

noting that CPA occurs when an eigenvalue of the scattering matrix goes to zero [32]. The scattering matrix can be constructed analytically from the transfer matrix or found numerically in full-wave solvers such as COMSOL [31]. In

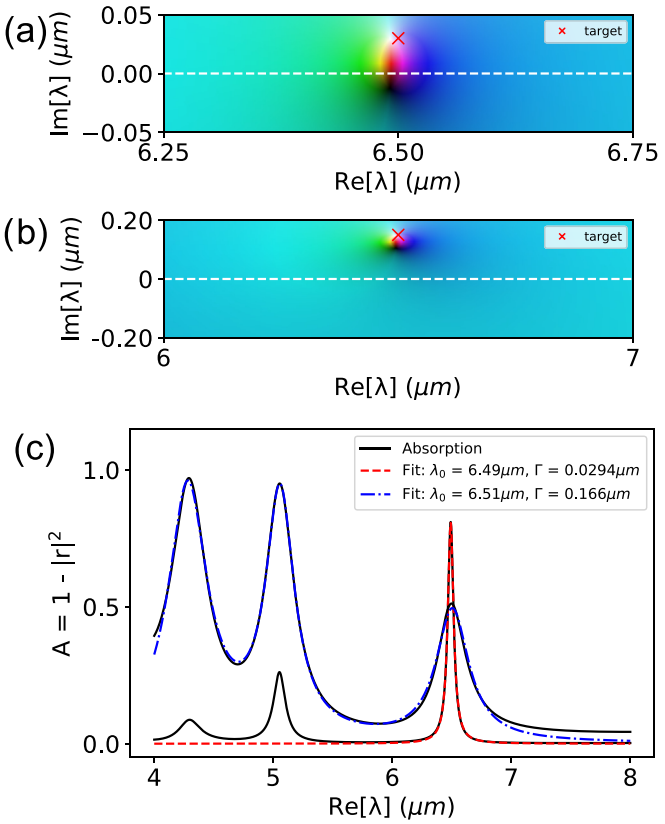

FIG. 3. The original absorbing stack, shown in Fig. 1(e), has been modified into two structures that contain a QNM at $\lambda_1 = (6.5 + 0.03i)$ μm and $\lambda_2 = (6.5 + 0.15i)$ μm, respectively. The former is close to the real axis, corresponding to a narrow bandwidth, while the latter has a broader bandwidth. Plotted on panels (a) and (b), respectively, are the reflection coefficients in the complex plane, showing that a QNM is indeed located at the chosen complex frequency. The absorption spectra of the two structures are plotted as a function of real wavelength (c). Fitted Lorentzians in dashed red (blue) correspond to fitting to the narrow (broad) resonance, verifying the complex frequencies of the QNMs. For the broadband case, we must fit a sum of three Lorentzians to accurately model the spectral profile, and obtain the correct fitting parameters.

Fig. 4 we plot the smallest eigenvalue of the scattering matrix of the slab as a function of frequency. A clear dip is seen at the desired frequency. We also show field profiles under incidence both from only one side and from both sides at different frequencies. Under incidence from only the left side, one can see the usual interference between reflected and incident field to the left of the slab and the constant transmitted field. Under excitation from both sides, but away from the target CPA frequency, one can see reflection from both sides. At the target CPA frequency of 125 MHz, an almost constant field amplitude is observed, indicating perfect absorption.

So far, all of the examples provided have been in one dimension. However, our method is straightforwardly extended to higher dimensions. To illustrate this we consider a two-dimensional (2D) square dielectric resonator, shown in Fig. 5(a). The resonator is a silicon cross inside a gallium arsenide square. To find how to change the permittivity to place a pole at a particular complex frequency, we must solve the eigenvalue problem Eq. (6) in two dimensions. To do this, we use COMSOL's coefficient form partial differential equation interface, which allows one to solve problems of the form

$$\lambda^2 e_a \phi - \lambda d_a \phi + \nabla \cdot (-c\nabla\phi - \alpha\phi + \gamma) + \beta\nabla\phi + a\phi = f, \tag{9}$$

where λ is the eigenvalue. Choosing the coefficients to be $e_a = 0, c = 1, d_a = 1,$ and $a = -k^2\varepsilon$, this becomes exactly the eigenvalue problem we would like to solve:

$$\nabla^2\phi + k^2\varepsilon\phi = -\lambda\phi, \tag{10}$$

where $\lambda = k^2\varepsilon_b$. The outgoing wave boundary condition can be applied to the outside edge of the resonator using the "flux/source" boundary condition. Generally, this boundary condition is

$$-\boldsymbol{n} \cdot (-c\nabla\phi + \alpha\phi + \gamma) = g - \phi u, \tag{11}$$

where $\boldsymbol{n}$ is a unit vector normal to the surface of the resonator at a given point. It is not necessary for $\boldsymbol{n}$ to be normal to the surface; it only needs to point outwards. With our parameter choices this becomes

$$\boldsymbol{n} \cdot \nabla\phi = -q\phi. \tag{12}$$

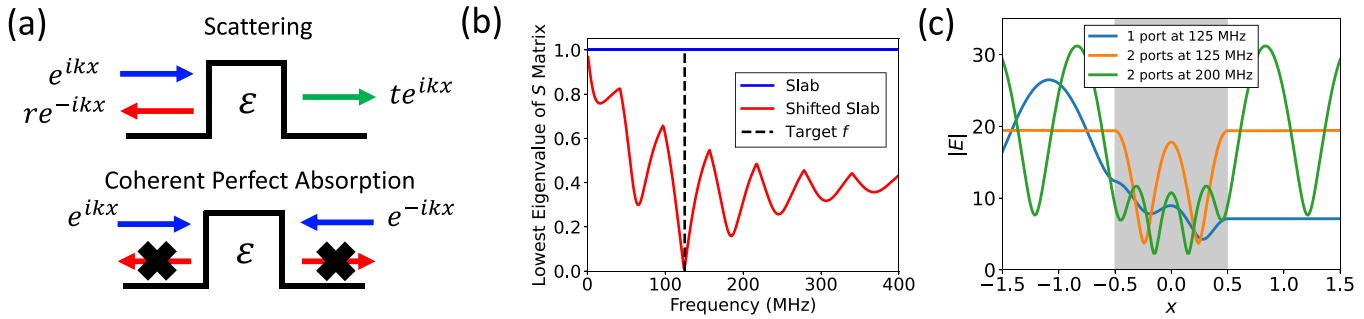

FIG. 4. An example of using our eigenpermittivity method to design a structure that exhibits coherent perfect absorption, shown schematically in (a). Under incidence from one direction, the structure scatters in the usual way, but under incidence from both sides reflection vanishes. We design a permittivity step of length $L = 1$ of permittivity $\varepsilon = \pi^2 + (-3.98 + i\ 1.59)$ that exhibits this behavior at the desired frequency of 125 MHz. To verify this, we show (b) the smallest eigenvalues of the scattering matrix of the structure. Vanishing eigenvalue indicates coherent perfect absorption. This can be clearly observed at the target frequency of 125 MHz. The fields (c) also indicate coherent perfect absorption. Under excitation from one side or off of the target frequency, reflections are observed. At the design frequency, there is a standing wave.

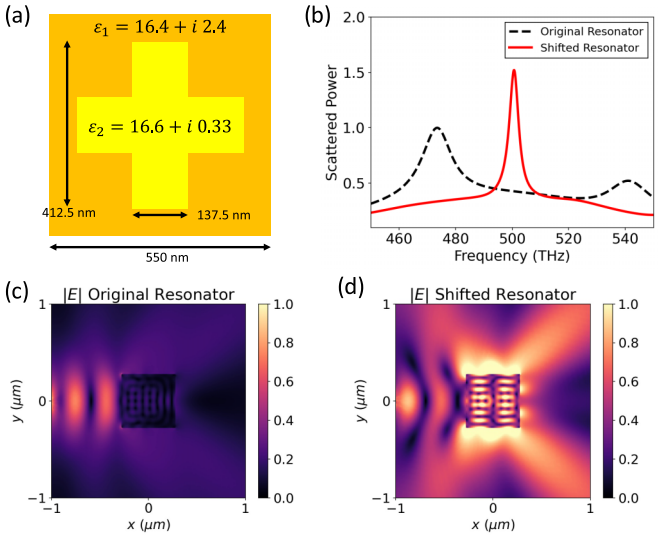

FIG. 5. An example of using our eigenpermittivity framework to place the quasinormal modes of a 2D resonator. The resonator, shown in the inset in panel (a), is made of two different permittivities, ε_1 (silicon at 550 nm) and ε_2 (gallium arsenide at 550 nm). We apply our framework to find a permittivity offset to move a pole to the complex frequency $(500 + 1i)$ THz. The background is $\varepsilon_b = -1.37 + i0.88$. To verify the location of the pole, we excite the resonator with a point electric dipole, located at $(-1100\,\text{nm}, 0)$, and calculate the total scattered power, shown in panel (b). A clear peak is present in the spectrum of the shifted structure at the desired frequency of 500 THz, which is not present in the spectrum of the unshifted structure. Examining the fields of the resonator driven by a nearby dipole at a frequency of 500 THz (c, d), we see that the excitation of the mode in the shifted structure greatly increases the scattering.

Setting $q = ik$ gives the correct outgoing boundary condition. Solving this eigenvalue problem for the 2D geometry shown in Fig. 5(a), and choosing the location of the pole to be $f = 500 + 1i$ THz, we find a background permittivity of $\varepsilon_b = -1.37 + i0.88$. To verify that a QNM is now located at the correct complex frequency, we excite the resonator with a nearby point dipole and examine the total scattered power before and after the permittivity shift is applied. This is shown in Fig. 5(b). Once the shift is applied, there is a clear peak in scattered power at the desired wavelength. Additionally, the fields when the resonator is driven at 500 THz are shown in Figs. 5(c) and 5(d). Once the permittivity of the resonator is shifted, scattering at the desired frequency is greatly enhanced by the presence of the QNM.

Although simple to implement, this eigenpermittivity method only allows one to choose the complex frequency of a single QNM. We now explore the possibility of applying an iterative method to move one or more QNMs to desired complex frequencies, by changing the spatial variation of the permittivity profile.

III. OPTIMIZATION APPROACH TO MOVING POLES

The second method we present to move QNMs to desired complex frequencies is to use an iterative procedure, based on perturbation theory. Standard Rayleigh-Schrödinger perturbation theory [33] of Hermitian quantum mechanics connects a change in the potential δV to a change in the nth energy level E_n through the matrix element:

$$\delta E_n = \langle \phi_n | \delta V | \phi_n \rangle, \tag{13}$$

where the states are normalized so that $\langle \phi_n | \phi_m \rangle = \delta_{nm}$. Usually the perturbation to the potential is known and the energy-level shifts are calculated, e.g., in the textbook analysis of the Stark effect (see [33] Sec. 76). Being able to analytically connect structure and function is the key to inverse design, allowing one to find derivatives of a quantity of interest (here, the energy) in terms of derivatives of the structure (the potential). With this observation, it is possible to use perturbation theory backwards to find how one should change the potential to get a particular energy level. This idea can be extended to move the complex frequency of a QNM of an electromagnetic resonator. Instead of a potential, we seek to design a permittivity profile $\varepsilon(x)$ that has a QNM, k_n, at a particular complex frequency. However, as QNMs grow in space, they cannot be normalized. The expressions that connect a change in the permittivity profile to a change in the complex wave number k_n require some modification. Regularization techniques have been used to develop a perturbation theory for QNMs in both quantum mechanics [34,35] and electromagnetism [36]. Perturbation theory can be used to connect a change in the permittivity $\delta\varepsilon(x)$ to a change in the complex frequency of the QNM [37] through

$$\delta k_n = \frac{1}{2k_n} \frac{\int_{-L/2}^{L/2} \phi_n^2(x) \delta\varepsilon(x) dx}{\langle \phi_n | \phi_n \rangle}, \tag{14}$$

where $k = k' + ik''$ and the inner product is now [35]

$$\langle \phi_n | \phi_n \rangle = \int_{-L/2}^{L/2} \phi_n^2(x) dx + i\big[\phi_n^2(-L/2) + \phi_n^2(L/2)\big]. \tag{15}$$

If we change the permittivity by a small amount $\Delta\varepsilon$ at a particular location x_i so that $\delta\varepsilon(x) = \Delta\varepsilon\delta(x - x_i)$, we find that

$$\delta k_n = \frac{1}{2k_n} \frac{\phi_n^2(x_i)\Delta\varepsilon}{\langle \phi_n | \phi_n \rangle}. \tag{16}$$

As this is true for all x_i, we can divide by the small change in permittivity to find the gradient of the wave number with respect to the permittivity:

$$\frac{\partial k_n}{\partial \varepsilon} = \frac{\phi_n^2(x)}{2k_n \langle \phi_n | \phi_n \rangle}. \tag{17}$$

Importantly, this gives a continuous function for the derivative of the complex frequency of the QNM with respect to the spatial structure of the permittivity. For example, say we would like to move mode k_n to the complex frequency $k_\star$. We can write a suitable figure of merit and its derivative as

$$\mathcal{F} = (k_n - k_\star)^2, \tag{18}$$

$$\frac{\partial \mathcal{F}}{\partial \varepsilon} = 2(k_n - k_\star) \frac{\partial k_n}{\partial \varepsilon}. \tag{19}$$

Updating the permittivity from iteration i to $i + 1$ is done according to

$$\varepsilon^{(i+1)}(x) = \varepsilon^{(i)}(x) + \gamma \frac{\partial \mathcal{F}}{\partial \varepsilon}, \tag{20}$$

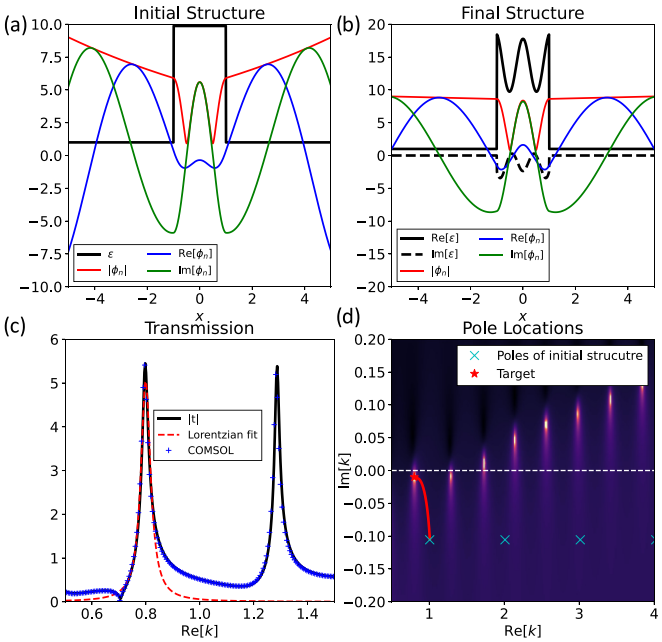

FIG. 6. An example of using our iterative method to move a pole to a desired location. Beginning from (a) a step of the dielectric which supports a QNM at $k = 1 - 0.1i$, our iterative method designs the permittivity distribution shown in panel (b), which supports a QNM at the desired frequency $k_\star = 0.8 - 0.01i$. The resulting transmission of the structure is shown in panel (c), and compared to a full-wave solver. Fitting a Lorentzian to the transmission peak associated with $k_\star$, we find that the peak is at $k_0 = 0.799$ with width $\Gamma = 0.0109$. The path of the pole over the optimization is shown in panel (d).

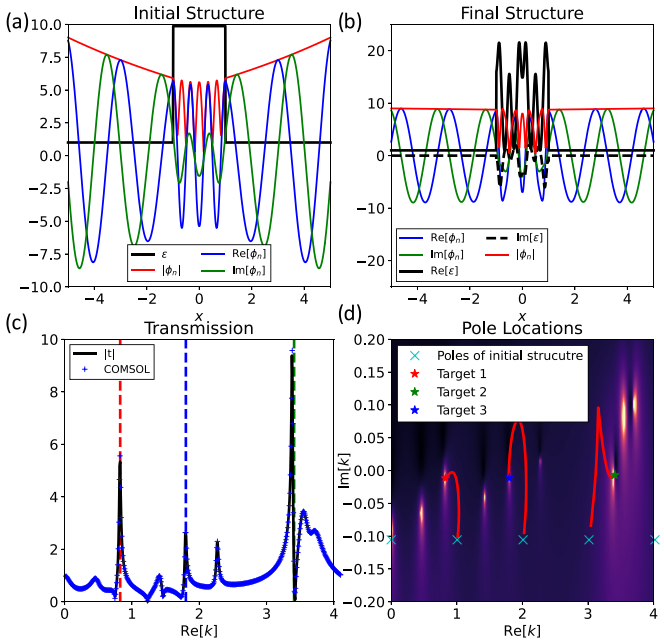

FIG. 7. An example of using the iterative method we present to move three poles to desired complex frequencies at the same time. Beginning from a permittivity step shown in panel (a), the real poles associated with $\mathrm{Re}[k] = 1, 2, 3$ are moved to the targets: $k_1 = 0.8 - 0.007i$, $k_2 = 3.5 - 0.008i$, and $k_3 = 1.8 - 0.009i$. The resulting permittivity profile is shown in panel (b) and its transmission coefficient is shown in panel (c). Clear peaks are seen at the three target values of k. The path of the poles over the optimization is shown in panel (d).

where γ is the step size. This makes the evaluation of the figure of merit gradients extremely efficient, similar to the adjoint method [38]. Combining this with gradient descent optimization [39], we have found how to update the permittivity distribution in order to arbitrarily change the complex frequencies of the QNMs.

An example of this procedure is shown in Fig. 6. We begin by selecting a QNM of the system: the frequency of which we want to modify. The complex wave number of this mode can be found by root finding in the complex plane, i.e., using Newton's method. Specifying a target frequency of the pole $k_\star$, then using Eqs. (17), (19), and (20) to iteratively update the permittivity distribution, allows the pole to be moved to the desired complex frequency. At every iteration, ϕ_n and k_n must be recalculated. In the example of Fig. 6 we move the pole originally at $k = 1 - 0.1i$ to $k_\star = 0.8 - 0.01i$, and show that this yields a structure with a peak in transmission at the designed frequency with the designed width. It should be noted that while we can move the pole to an arbitrary complex frequency, complete control of both the real and imaginary parts of the permittivity is required.

As another example of this method, we consider trying to move several poles simultaneously. In Fig. 7 we take the poles originally at $k = 1 - 0.1i$, $2 - 0.1i$, and $3 - 0.1i$ and move them to three different values k_1, k_2, and k_3. Interestingly, due to the presence of other nearby poles, the transmission profile of the resulting structure becomes more complex, however clear narrow transmission peaks associated with k_1, k_2, and k_3 are evident. If one controls all poles of interest over a given range of k values, almost complete control over the transmission profile can be obtained.

IV. CONCLUSIONS AND OUTLOOK

In this paper we address the inverse design problem: "how should one change a photonic system to ensure a quasinormal mode appears at a predetermined complex frequency?". We propose two approaches to answer this question. The first is to reexpress the permittivity of a system as the original permittivity profile, plus some global background shift $\varepsilon_s(x) + \varepsilon_b$. This allows us to write the Helmholtz equation as an eigenvalue problem for the background permittivity ε_b. By choosing a target complex frequency, we can find a (complex) background permittivity that can be added to the structure so that a QNM occurs at the desired complex frequency with the desired linewidth. This method could be used to modify existing structures to control the frequency and bandwidth of a resonant system. We also show that we can apply this method in order to construct materials that, at a single frequency of operation, act as coherent perfect absorbers.

The second approach we develop is an iterative procedure based on perturbation theory: a small change in permittivity can be connected to the shift in complex frequency of a QNM. By defining a suitable figure of merit, and combining with gradient descent optimization, we can iteratively change the

spatial permittivity profile to move a QNM closer to a target frequency. This procedure can also be used to move multiple QNMs to different target frequencies. This iterative approach can be further modified in many ways, for example, by restricting the search space of $\delta\varepsilon$ to only allow loss rather than gain, or to ensure $\varepsilon(x) > 1$. Also, rather than manipulating the full spatial form of ε, we could seek to change only a few free parameters such as width and height of the dielectric step.

The approaches we have developed open up several avenues of exploration to design, for example, broadband absorbers for solar cells and thermal emitters. Since the framework also applies to leaky waveguides, our methods could also be used to design leaky-wave antennas. Rather than manually changing structural parameters until a QNM appears at the correct complex frequency, the methods we present leverage the benefits of inverse design to rapidly design materials that have the desired properties. Importantly, as our methods allow QNMs to be placed exactly, both resonance frequency and linewidth can be tuned with a high degree of accuracy.

All data and code created during this research are openly available from the corresponding authors, upon reasonable request.

ACKNOWLEDGMENTS

The authors would like to thank Josh Glasbey and Ian Hooper for many illuminating discussions and Jake Binsley for his assistance with Blender. We acknowledge financial support from the Engineering and Physical Sciences Research Council (EPSRC) of the United Kingdom, via the EPSRC Centre for Doctoral Training in Metamaterials (Grant No. EP/L015331/1). J.R.C. also wishes to acknowledge financial support from Defence Science Technology Laboratory. S.A.R.H. acknowledges financial support from the Royal Society (Grant No. URFR211033).

[1] G. Gamow, Zur quantentheorie des atomkernes, Z. Phys. **51**, 204 (1928).
[2] H. A. Bethe, Nuclear physics B: Nuclear dynamics, theoretical, Rev. Mod. Phys. **9**, 69 (1937).
[3] S. Chandrasekhar and S. Detweiler, The quasi-normal modes of the Schwarzschild black hole, Proc. R. Soc. A **344**, 441 (1975).
[4] P. T. Kristensen, K. Herrmann, F. Intravaia, and K. Busch, Modeling electromagnetic resonators using quasinormal modes, Adv. Opt. Photon. **12**, 612 (2020).
[5] A. K. Ghatak, Leaky modes in optical waveguides, Opt. Quantum Electron. **17**, 311 (1985).
[6] J. Hu and C. R. Menyuk, Understanding leaky modes: Slab waveguide revisited, Adv. Opt. Photon. **1**, 58 (2009).
[7] F. Alpeggiani, N. Parappurath, E. Verhagen, and L. Kuipers, Quasinormal-Mode Expansion of the Scattering Matrix, Phys. Rev. X **7**, 021035 (2017).
[8] S. G. Tikhodeev, A. L. Yablonskii, E. A. Muljarov, N. A. Gippius, and T. Ishihara, Quasiguided modes and optical properties of photonic crystal slabs, Phys. Rev. B **66**, 045102 (2002).
[9] L. Zschiedrich, F. Binkowski, N. Nikolay, O. Benson, G. Kewes, and S. Burger, Riesz-projection-based theory of light-matter interaction in dispersive nanoresonators, Phys. Rev. A **98**, 043806 (2018).
[10] J. Yang, H. Giessen, and P. Lalanne, Simple analytical expression for the peak-frequency shifts of plasmonic resonances for sensing, Nano Lett. **15**, 3439 (2015).
[11] S. Both, M. Schöferling, F. Sterl, E. A. Muljarov, H. Giessen, and T. Weiss, Nanophotonic chiral sensing: How does it actually work?, ACS Nano **16**, 2822 (2022).
[12] A. Sakurai, K. Yada, T. Simomura, S. Ju, M. Kashiwagi, H. Okada, T. Nagao, K. Tsuda, and J, Shiomi, Ultranarrow-Band Wavelength-Selective Thermal Emission with Aperiodic Multilayered Metamaterials Designed by Bayesian Optimization, ACS Cent. Sci. **5**, 319 (2019).
[13] M. De Zoysa, T. Asano, K. Mochizuki, A. Oskooi, T. Inoue, and Susumu Noda, Conversion of broadband to narrowband thermal emission through energy recycling, Nat. Photonics **6**, 535 (2012).
[14] N. Liu, M. Mesch, T. Weiss, M. Hentschel, and H. Giessen, Infrared perfect absorber and its application as plasmonic sensor, Nano Lett. **10**, 2342 (2010).
[15] N. I. Landy, S. Sajuyigbe, J. J. Mock, D. R. Smith, and W. J. Padilla1, Perfect Metamaterial Absorber, Phys. Rev. Lett. **100**, 207402 (2008).
[16] S. Luo, J. Zhao, D. Zuo, and X. Wang, Perfect narrow band absorber for sensing applications, Opt. Express **24**, 9288 (2016).
[17] A. Lochbaum, Y. Fedoryshyn, A. Dorodnyy, U. Koch, C. Hafner, and J. Leuthold, On-chip narrowband thermal emitter for mid-ir optical gas sensing, ACS Photonics **4**, 1371 (2017).
[18] K. Aydin, V. E. Ferry, R. M. Briggs, and H. A. Atwater, Broadband polarization-independent resonant light absorption using ultrathin plasmonic super absorbers, Nat. Commun. **2**, 517 (2011).
[19] R. A. Pala, J. White, E. Barnard, J. Liu, and M. L. Brongersma, Design of plasmonic thin-film solar cells withbroadband absorption enhancements, Adv. Mater. **21**, 3504 (2009).
[20] Y. Zhou, Z. Qin, Z. Liang, D. Meng, H. Xu, D. R. Smith, and Y. Liu, Ultra-broadband metamaterial absorbers from long to very long infrared regime, Light Sci. Appl. **10**, 138 (2021).
[21] F. Ding, J. Dai, Y. Chen, J. Zhu, Y. Jin, and S. I. Bozhevolnyi, Broadband near-infrared metamaterial absorbers utilizing highly lossy metals, Sci. Rep. **6**, 39445 (2016).
[22] V. Grigoriev, A. Tahri, S. Varault, B. Rolly, B. Stout, J. Wenger, and N. Bonod, Optimization of resonant effects in nanostructures via weierstrass factorization, Phys. Rev. A **88**, 011803 (2013).
[23] T. Wu, A. Baron, P. Lalanne, and K. Vynck, Intrinsic multipolar contents of nanoresonators for tailored scattering, Phys. Rev. A **101**, 011803 (2020).
[24] X. Ming and L. Sun, Optimization of broadband perfect absorber by weierstrass factorization, IEEE Photonics J. **11**, 4602010 (2019).

[25] W. Yan, P. Lalanne, and M. Qiu, Shape Deformation of Nanoresonator: A Quasinormal-Mode Perturbation Theory, Phys. Rev. Lett. **125**, 013901 (2020).

[26] A. Sommerfeld, *Partial Differential Equations in Physics* (Academic, New York, 1949).

[27] F. J. Zerilli, Effective Potential for Even-Parity Regge-Wheeler Gravitational Perturbation Equations, Phys. Rev. Lett. **24**, 737 (1970).

[28] P. L. Kapur and R. Peierls, The dispersion formula for nuclear reactions, Proc. R. Soc. A **166**, 277 (1938).

[29] P. Lalanne, W. Yan, A. Gras, C. Sauvan, J.-P. Hugonin, M. Besbes, G. Demésy, M. D. Truong, B. Gralak, F. Zolla, A. Nicolet, F. Binkowski, L. Zschiedrich, S. Burger, J. Zimmerling, R. Remis, P. Urbach, H. T. Liu, and T. Weiss, Quasinormal mode solvers for resonators with dispersive materials, J. Opt. Soc. Am. A **36**, 686 (2019).

[30] P. Y. Chen, D. J. Bergman, and Y. Sivan, Generalizing Normal Mode Expansion of Electromagnetic Green's Tensor to Open Systems, Phys. Rev. Appl. **11**, 044018 (2019).

[31] COMSOL Multiphysics® v. 6.0. www.comsol.com, COMSOL AB, Stockholm, Sweden.

[32] Y. D. Chong, L. Ge, H. Cao, and A. D. Stone, Coherent Perfect Absorbers: Time-Reversed Lasers, Phys. Rev. Lett. **105**, 053901 (2010).

[33] L. D. Landau and E. M. Lifshitz, *Quantum Mechanics: Non-Relativistic Theory*, 2nd ed. (Pergamon, New York, 1965).

[34] Y. B. Zel'Dovich, On the theory of unstable states, Sov. Phys. JETP **12**, 3 (1961).

[35] P. T. Leung, Y. T. Liu, W. M. Suen, C. Y. Tam, and K. Young, Logarithmic perturbation theory for quasinormal modes, J. Phys. A **31**, 3271 (1998).

[36] E. A. Muljarov, W. Langbein, and R. Zimmermann, Brillouin-Wigner perturbation theory in open electromagnetic systems, Europhys. Lett. **92**, 50010 (2010).

[37] A. M. Perelomov and Y. B. Zel'Dovich, *Quantum Mechanics: Selected Topics* (World Scientific, Singapore, 1998).

[38] C. M. Lalau-Keraly, S. Bhargava, O. D. Miller, and E. Yablonovitch, Adjoint shape optimization applied to electromagnetic design, Opt. Express **21**, 21693 (2013).

[39] W. H. Press, S. A. Teukolsky, W. T. Vetterling, and B. P. Flannery, *Numerical Recipes: The Art of Scientific Computing*, 3rd ed. (Cambridge University, New York, 2007).